Vol. 91 No. 2 pp. 486–499 ACTA GEOLOGICA SINICA (English Edition) Apr. 2017

Early Crystallized Titanomagnetite from Evolved Magmas and Magma Recharge in the Mesoproterozoic Zhuqing Oxide-Bearing Gabbroic Intrusions, Sichuan, SW China

FAN Hongpeng and ZHU Weiguang*

State Key Laboratory of Ore Deposit Geochemistry, Institute of Geochemistry, Chinese Academy of Sciences, Guiyang 550081, Guizhou, China

Abstract: The ca. 1.5 Ga mafic intrusions in the Zhuqing area, predominantly composed of alkaline gabbroic rocks in the Kangdian region of SW China, occur as dykes or irregular small intrusions hosting Fe–Ti–V mineralization. All of the intrusions that intrude the dolomite or shales of the Mesoproterozoic Heishan Formation of the Huili Group are composed of three cyclic units from the base upward: a marginal cyclic unit, a lower cyclic unit and an upper cyclic unit. The Fe–Ti–V oxide ore bodies are hosted in the lower and upper cyclic units. The textural relationships between minerals in the intrusions suggest that titanomagnetite formed earlier than silicate grains because euhedral magnetite and ilmenite grains were enclosed in clinopyroxene and plagioclase. Both the magnetite$_{ss}$–ilmenite$_{ss}$ intergrowths due to subsolidus oxidation–exsolutions and the relative higher V distribution coefficient between magnetite and silicate melts in the gabbros from the Zhuqing area are different from those of other typical Fe–Ti bearing mafic rocks, suggesting that the oxygen fugacity was low in the gabbric rocks from the Zhuqing area. This finding was further confirmed by calculations based on the compositions of magnetite and ilmenite pairs. The clinopyroxene, magnetite and ilmenite in the intrusions from the Zhuqing area had considerably lower MgO than those of other typical Fe–Ti oxide-rich complexes, suggesting that the titanomagnetite from the intrusion may have crystallized at a relatively late stage of evolution from a more evolved magma. Titanomagnetite first fractionally crystallized and subsequently settled in the lower parts of the magma chamber, where it concentrated and formed Fe–Ti–V oxide ore layers at the bases of the lower and upper cycles. Moreover, the occurrence of multiple Fe-Ti oxide layers alternating with Fe-Ti oxide-bearing silicate layers suggests that multiple pulses of magma were involved in the formation of the intrusions and related Fe-Ti-V oxide deposits in the Zhuqing area.

Key words: Fe–Ti oxide, mineral chemistry, patrogenesis, Mesoproterozoic Zhuqing oxide ore deposits, Kangdian region, SW china, East margin of Tibetan Plateau, Proto-Tethys

1 Introduction

The mechanism of magnetite crystallization in Fe–Ti oxide ore deposits has long been debated. One proposal is that Fe–Ti oxides are precipitated from immiscible Fe-rich melts from silicate magma at the late stage (Lister, 1966; Philpotts, 1967; Reynolds, 1985a; Zhou et al., 2005; 2013; Dong et al., 2013; Wang and Zhou, 2013; Shi et al., 2014). Alternatively, the settling and sorting of early cumulus Fe–Ti oxides may play an important role in the generation of Fe–Ti oxide ores (Charlier et al., 2006; Pang et al., 2008; Wang et al., 2008; Ganino et al., 2008; Bai et al., 2012; Howarth et al., 2013; Howarth and Prevec, 2013). The former model has been disproven by experiments showing that immiscible Fe–Ti oxide melts would contain a large proportion of phosphorus (Philpotts, 1967) and SiO_2 (Veksler et al., 2007) and the fact that the contents of apatite and silica in certain types of ore is relatively low (e.g., Bai et al.,2012; Pang et al., 2010). Fe–Ti oxides usually crystallized later to form the Fe–Ti oxide layers that commonly occur in the upper parts of large layered intrusions in the world, such as the Bushveld Complex (Reynolds, 1985b), the Skaergaard intrusion (McBirney, 1996), and the Muskox intrusion (Irvine, 1988). However, it had been suggested that magnetite may crystallize at an early stage from magma with a relatively high oxygen

* Corresponding author. E-mail: zhuweiguang@vip.gyig.ac.cn

fugacity (fO_2) (Toplis and Caroll 1995; Ganino et al. 2008; Pang et al. 2010; Bai et al. 2012). The early crystallization and accumulation of Fe–Ti oxides, while phosphorus remained in the melt and crystallized only at higher degrees of magma differentiation, can indeed explain the presence of apatite-rich layers in the upper sequence of the gabbros from the world-class Fe–Ti–V deposits in the Panxi region of SW China (Bai et al., 2012; Dong et al., 2013; Howarth et al., 2013; Wang and Zhou, 2013). Moreover, it has been suggested that the early crystallization of the Fe–Ti oxides could have been induced by the initial Fe–Ti-rich composition of the parental magma (Zhou et al., 2008; Bai et al., 2012) or by the higher oxygen fugacity in the magma (Ganino et al., 2008, 2013a, b; Bai et al., 2012; Pêcher et al., 2013; Howarth et al., 2013) or even by fractionation of H_2O (Xing et al., 2012). Therefore, the difficulty in elucidating the Fe-Ti mineralization process is in determining the timing of crystallization and the controlling factors of the Fe–Ti oxides.

The ca. 1.5 Ga intrusions in the Zhuqing area contain Fe–Ti–V oxide ore deposits with over 100 Mt of ore reserves in three intrusive bodies. The rest of the intrusions in the region also have Fe–Ti–V oxide mineralization potential and were likely the products of a mantle plume that contributed to the break-up of the Paleo- to Mesoproterozoic supercontinent Columbia (Fan et al. 2013). The gabbroic intrusions in the Zhuqing area that host Fe–Ti oxide ore were likely crystallized in a close magma system (Fan et al., 2013), offering a good opportunity for investigating crystallization of the Fe–Ti oxides. In this paper, we present the mineral compositions of clinopyroxene and Fe–Ti oxides (magnetite and ilmenite), as determined by electron microprobe, for Fe–Ti oxide ore-bearing mafic intrusions in the Zhuqing area with the aim of further elucidating the mechanism of Fe–Ti oxide crystallization and accumulation.

2 Geological Settings

2.1 Regional geology

The South China Block consists of two major Precambrian blocks: the Yangtze Block to the northwest and the Cathaysia Block to the southeast (present coordinates) (Fig. 1a). Rocks > 2900 Ma are sparse in the northern part of the Yangtze Block (Gao et al. 2001). However, there are ancient lower crustal xenoliths (Zheng et al. 2006) and abundant Archean to Paleoproterozoic detrital zircons in the Meso- to Neoproterozoic sedimentary sequences (Sun et al. 2009; Zhao et al. 2010; Wang et al. 2013), suggesting widespread Archean to Paleoproterozoic basement rocks. Widely distributed Proterozoic strata are thought to be the typical folded basement of the Yangtze Block (Yang et al., 2005, 2012; Peng et al., 2009; Hou et al., 2013; Ye et al., 2013; Zhou et al., 2014; Song and Song, 2015) and these strata are uncomfortably overlain by an unmetamorphosed Sinian to Cenozoic cover sequence (Yan et al. 2003).

The Kangdian area is located near the western margin of the Yangtze Block, South China (Fig. 1a). The oldest supracrustal rocks in this area are the late Paleo- to Mesoproterozoic meta-volcanic and sedimentary rocks, termed the Dahongshan Group (Greentree and Li 2008), the Dongchuan Group (Zhao et al. 2010), the Hekou Group (Zhao and Zhou 2011), the Huili Group (Yin et al. 2011), and the Kunyang Group (Yin et al. 2011), occur along the Luzhijiang fault and a series of related NNE-trending faults (Fig. 1b). These rocks consist of meta-sedimentary rocks interbedded with felsic and mafic meta-volcanic rocks. For example, the Dahongshan, Hekou, Dongchuan, and Huili Groups contain mafic intrusions and meta-volcanic layers with zircon U–Pb ages of 1.5–1.7 Ga (Chang et al. 1997; Greentree and Li 2008; He 2009; Zhao et al. 2010; Zhao and Zhou 2011; Fan et al. 2013), and the Huili and Upper Kunyang Groups have meta-volcanic layers with zircon U–Pb ages of ~1.0 Ga (Chang et al. 1997; Mou et al. 2003; Greentree et al. 2006; Geng et al. 2007; Zhang et al. 2007). These rocks are overlain by a thick sequence (> 9 km) of Neoproterozoic (850–540 Ma) to Permian strata composed of clastic, carbonate and volcanic rocks.

A number of mafic intrusions intrude the dolomite and slate of the Mesoproterozoic Heishan Formation of the Huili Group in the Tong'an area of SW China (Fig. 1b). These intrusions, predominantly composed of alkaline gabbroic rocks, were distributed as dykes or irregular small intrusions bounded by a series of faults in the northeast of the Tong'an area (Fig. 1b).

2.2 Petrography of the intrusions in the Zhuqing area

The mafic intrusions in the Zhuqing area are of variable sizes, up to 4 km long and commonly 90–370 m width, striking NW 303°–349° and dipping ~45°–65° to southwest with an average thickness of ~170 M. The Fe–Ti–V oxide ore-bearing deposits are hosted in the lower zones of two gabbric intrusions in the Zhuqing area (Fig. 1b). The ore bodies with over 100 Mt ore reserves are arranged in parallel stratiforms, lenticulars or veins interbedded with 1 to 2 thin gabbric layers or Lens (Fig. 2). Most of the intrusions consisting of medium- to coarse-grained gabbros (Figs. 3a and 3b), and the mineral grains are typically larger in the lower zone than those in the upper zone of the intrusions (Fig. 2b). These gabbros could be divided into oxide-rich and oxide-poor gabbros based on the whole-rock Fe_2O_3 content. The oxide-rich

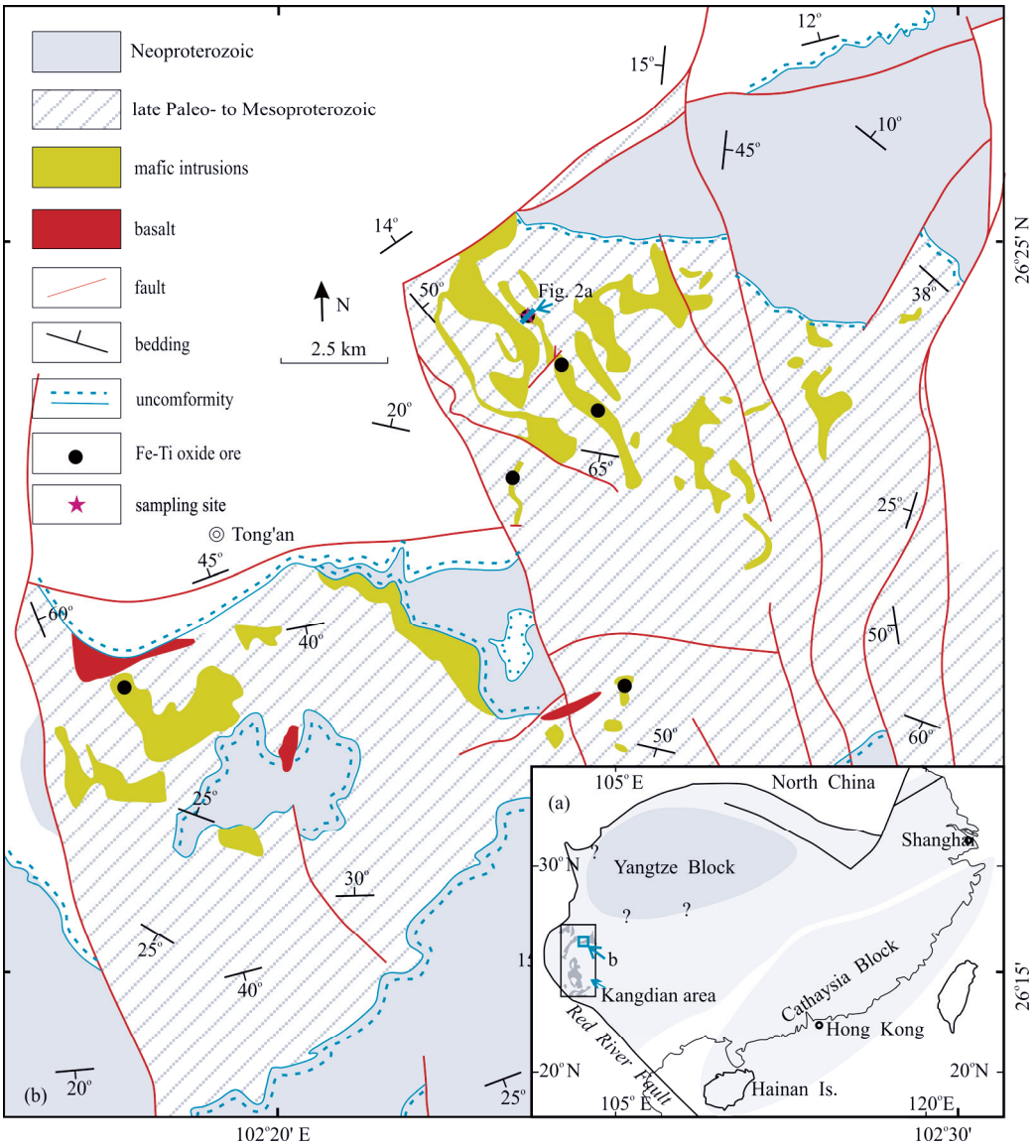

Fig. 1. (a) Simplified tectonic map showing the study area in relation to South China's major tectonic units (Li et al., 2007); (b) geological map of the Tong'an area showing mafic rocks including the intrusions in the Zhuqing area and sampling locations.

gabbros (Fe_2O_3 > 29 wt%) consist of >20 vol% Fe–Ti oxides (magnetite and ilmenite), approximately 40 vol% plagioclase, 30 vol% clinopyroxene, and minor amounts of hornblende, biotite and sulfide minerals; whereas the oxide-poor gabbros contain 40–60 vol% plagioclase, 30–40 vol% clinopyroxene, 5–10 vol% Fe–Ti oxides and minor amounts of sulfide minerals, apatite, hornblende and biotite. The textural relationships between minerals in the intrusions suggest that titanomagnetite formed earlier than the silicate grains because euhedral magnetite and ilmenite grains were enclosed in clinopyroxene and plagioclase (Figs. 3c and 3d). The magnetites in the gabbros of the Zhuqing area have ilmenite exsolutions with different shapes, such as trellis-shaped lamellae, which occur primarily in the cores of the host grains (Fig. 3f), and coarse-grained, which presents mostly at the rim of magnetite (Figs. 3g and 3h). The intrusions in the Zhuqing area can be divided into three cycles from the base to the top: a marginal cycle (zone 1), a lower cycle (zones 2 and 3), and an upper cycle (zones 4 and 5) (Fig. 2). The marginal cycle, located at the base of the intrusions, is mainly composed of coarse grains of plagioclase, clinopyroxene, Fe–Ti oxides, and minor amounts of apatite. The lower cycle is composed of a Fe–Ti oxide cumulated layer interbedded with thin gabbroic layers (zone 2) and an overlying medium- to coarse-grained gabbroic layer (zone 3). The upper cycle was similar to the lower cycle except that mineral grains were smaller in the upper cycle and apatite and sulfide minerals were present of in zone 5 of the upper cycle (Fig. 2).

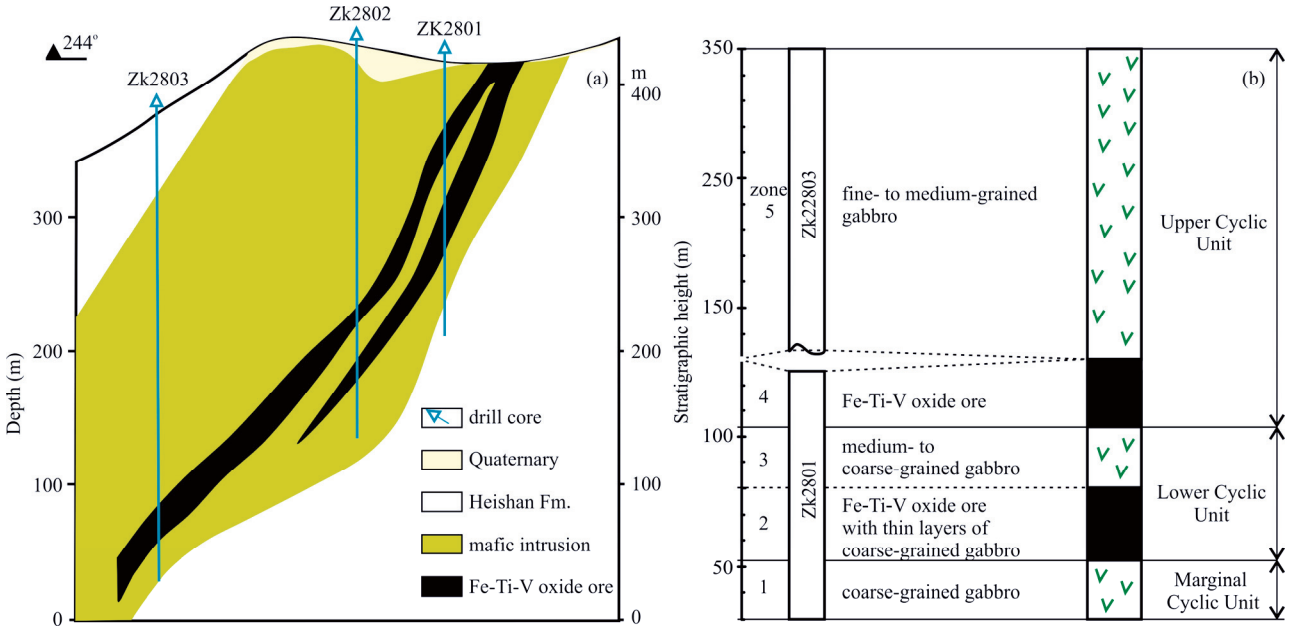

Fig. 2. The cross-section (a) and stratigraphic section (b) of the gabbros in the Zhuqing area, the position of the section is shown in Fig. 1b.

3 Sampling and Methods

In this study, twenty-three samples were collected from the drill core ZK2801; the sampling position is shown in Fig. 1b.

The compositions of clinopyroxene (Table 1) were analyzed using an EPMA-1600 electron microprobe wavelength-dispersive spectrometer at the State Key Laboratory of Ore Deposit Geochemistry (SKLODG), Institute of Geochemistry, Chinese Academy of Sciences (CAS). Analytical conditions were 25 nA beam current with acceleration voltage of 25 kV and beam size of 1 μm. The compositions of magnetite (Table 2) and ilmenite (Table 3) were determined using a JXA-8100 electron

Table 1 Average compositions (wt%) of clinopyroxene in gabbros from drill core Zk2801 in the intrusions from the Zhuqing area

Sample No.	ZK2834	ZK2830	ZK2828	ZK2826	ZK2823	ZK2818	ZK2814	ZK2811	ZK2809	ZK2808	ZK2807	ZK2806	ZK2804	ZK2802	ZK2801
Rock name	Gab	Gab	Gab	Ore	Ore	Ore	Gab	Gab	Gab	Gab	Gab	Gab	Ore	Ore	Ore
Unit	1	1	1	2	2	2	2	2	2	2	3	3	4	4	4
n	4	5	5	5	5	5	4	4	4	5	4	5	4	5	5
SiO_2	52.45	52.09	51.49	55.39	54.80	54.20	52.47	51.96	53.37	52.70	53.48	52.45	54.44	55.54	54.61
TiO_2	0.08	0.12	0.19	0.05	0.08	0.03	0.14	0.03	0.07	0.18	0.09	0.07	0.09	0.05	0.04
Al_2O_3	1.58	1.61	1.98	0.64	0.97	1.01	2.21	2.35	1.11	1.66	1.49	2.27	0.86	0.92	1.01
Cr_2O_3	0.00	0.01	0.01	0.03	0.00	0.01	0.00	0.02	0.00	0.01	0.02	0.01	0.03	0.02	0.02
MgO	8.97	7.44	7.45	13.80	13.53	13.21	9.80	9.45	9.60	9.29	10.07	8.85	11.39	12.23	11.99
CaO	11.41	11.47	11.52	12.13	12.27	11.88	11.52	11.60	11.83	11.53	11.90	11.34	11.78	12.03	11.77
MnO	0.37	0.21	0.36	0.15	0.17	0.17	0.32	0.23	0.23	0.35	0.30	0.26	0.17	0.15	0.19
FeO	24.91	27.10	27.58	17.11	17.63	17.46	22.91	23.22	23.62	24.16	22.66	24.52	20.12	19.51	19.76
Na_2O	0.45	0.34	0.36	0.25	0.32	0.28	0.61	0.46	0.24	0.41	0.34	0.53	0.30	0.30	0.33
K_2O	0.11	0.08	0.12	0.02	0.03	0.04	0.08	0.19	0.05	0.10	0.17	0.14	0.04	0.03	0.04
Total	100.32	100.47	101.06	99.56	99.80	98.29	100.06	99.51	100.12	100.38	100.52	100.43	99.22	100.78	99.77
$Mg^{\#}$	39.08	32.87	32.52	58.97	57.77	57.41	43.14	42.02	41.97	40.64	44.18	39.11	50.18	52.77	51.97
Si	2.054	2.062	2.026	2.116	2.090	2.101	2.041	2.037	2.089	2.058	2.070	2.048	2.119	2.119	2.106
Ti	0.002	0.004	0.006	0.001	0.002	0.001	0.004	0.001	0.002	0.005	0.003	0.002	0.003	0.001	0.001
Al	0.073	0.075	0.092	0.029	0.044	0.046	0.101	0.109	0.051	0.076	0.068	0.104	0.039	0.041	0.046
Cr	0.000	0.000	0.000	0.001	0.000	0.000	0.000	0.001	0.000	0.000	0.001	0.000	0.001	0.001	0.001
Mg	0.524	0.439	0.437	0.786	0.769	0.763	0.568	0.552	0.560	0.541	0.582	0.515	0.661	0.695	0.689
Ca	0.479	0.486	0.486	0.496	0.501	0.493	0.480	0.487	0.496	0.482	0.494	0.474	0.491	0.492	0.486
Mn	0.012	0.007	0.012	0.005	0.005	0.006	0.011	0.008	0.008	0.012	0.010	0.009	0.006	0.005	0.006
Fe^{3+}	0.000	0.000	0.000	0.000	0.000	0.000	0.000	0.000	0.000	0.000	0.000	0.000	0.000	0.000	0.000
Fe^{2+}	0.816	0.897	0.908	0.547	0.562	0.566	0.745	0.761	0.773	0.789	0.735	0.801	0.655	0.622	0.637
Na	0.034	0.026	0.027	0.019	0.024	0.021	0.046	0.035	0.018	0.031	0.026	0.040	0.023	0.022	0.025
K	0.005	0.004	0.006	0.001	0.001	0.002	0.004	0.010	0.002	0.005	0.008	0.007	0.002	0.001	0.002
Total	4.000	4.000	4.000	4.000	4.000	4.000	4.000	4.000	4.000	4.000	4.000	4.000	4.000	4.000	4.000
En	28.61	24.00	23.72	42.86	41.84	41.75	31.05	30.54	30.49	29.65	31.96	28.64	36.46	38.33	37.89
Fs	45.24	49.42	49.92	30.07	30.88	31.26	41.89	42.52	42.50	43.90	40.89	44.99	36.44	34.57	35.37
Wo	26.15	26.59	26.36	27.07	27.27	26.99	26.61	26.94	27.01	26.45	27.15	26.37	27.10	27.10	26.73

Note: Gab = oxide-poor gabbro; Ore = oxide-rich gabbro; n = number of analysis.

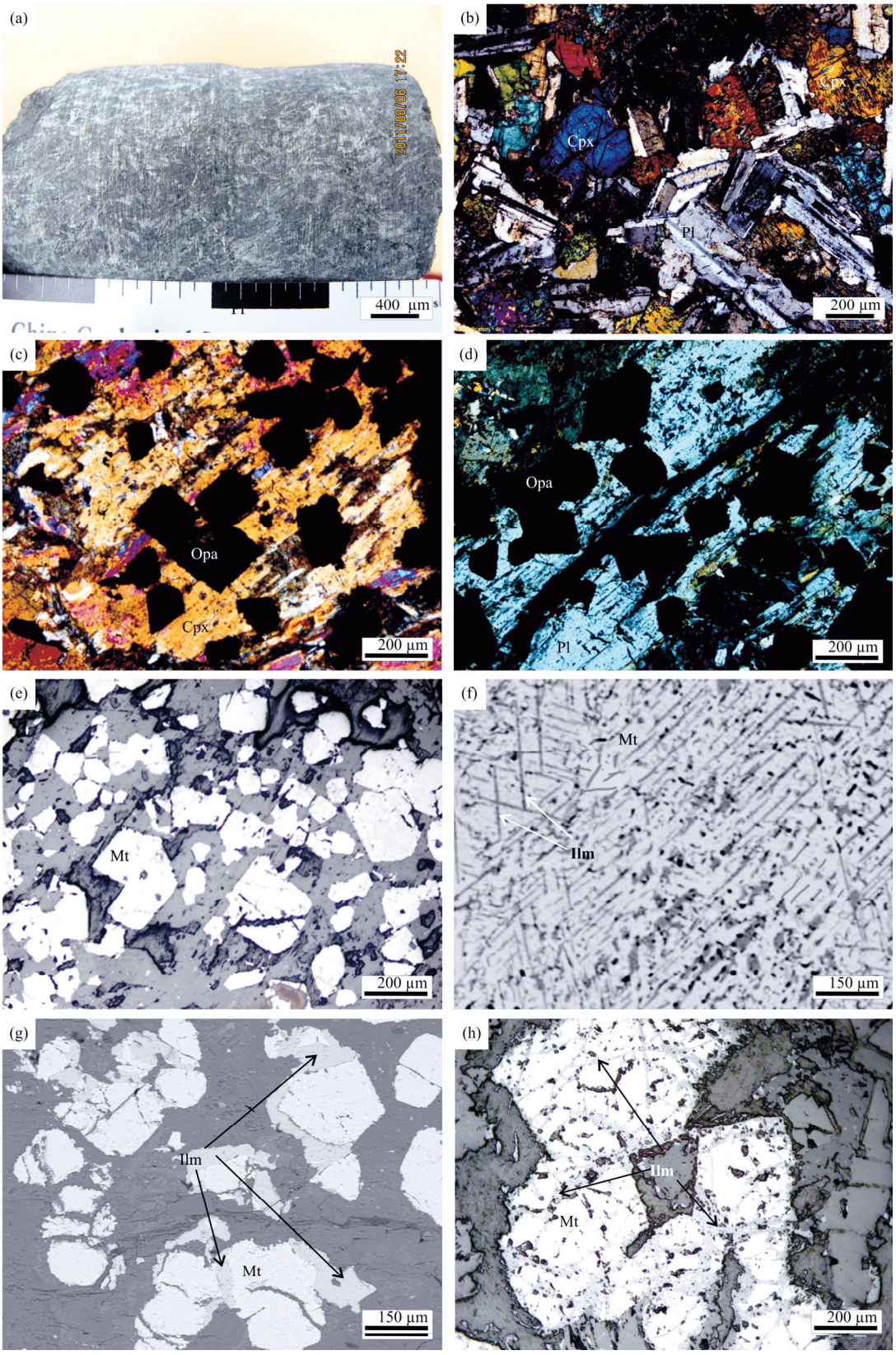

Fig. 3. Hand specimen and microscopic photographs and BSE images of the gabbros in the Zhuqing area.
(a) Sample from drill core showing the gabbroic structure; (b) microphotographs of minerals with gabbroic structure; euhedral magnetite and ilmenite grains enclosed in clinopyroxene (c) and plagioclase (d); (e) microphotographs of Fe–Ti rich gabbros; (f) trellis-shaped ilmenite exsolutions in the cores of the host magnetite; (g) and (h) coarse-grained ilmenite presented at the rim of magnetite. Pl = plagioclase; Cpx = clinopyroxene; Mt = magnetite; Ilm = ilmenite; Opa = Magnetite/Ilmenite.

Table 2 Average compositions (wt%) of magnetite in gabbros from drill core Zk2801 in the intrusions from the Zhuqing area

Sample No.	ZK 2834	ZK 2830	ZK 2827	ZK 2825	ZK 2823	ZK 2822	ZK 2821	ZK 2818	ZK 2817	ZK 2816	ZK 2813	ZK 2811	ZK 2807	ZK 2806	ZK 2805	ZK 2804	ZK 2802	ZK 2801
Rock name	Gab	Gab	Gab	Ore	Ore	Ore	Ore	Ore	Ore	Ore	Gab	Gab	Gab	Gab	Ore	Ore	Ore	Ore
Unit	1	1	1	2	2	2	2	2	2	2	3	3	3	3	4	4	4	4
n	4	5	3	2	8	7	6	1	2	5	2	6	6	5	2	4	8	7
MgO	0.02	0.02	0.04	0.02	0.01	0.02	0.04	0.00	0.05	0.01	0.00	0.02	0.02	0.02	0.01	0.02	0.03	0.03
Al_2O_3	0.01	0.01	0.06	0.02	0.03	0.04	0.03	0.04	0.03	0.04	0.04	0.03	0.03	0.03	0.03	0.03	0.06	0.04
TiO_2	30.21	19.64	20.65	13.97	17.77	19.69	18.24	8.86	12.67	14.25	16.71	24.00	24.63	24.63	21.34	17.47	8.90	22.62
FeO	56.52	47.82	48.3	42.79	46.27	47.99	46.78	38.92	42.11	43.6	45.04	51.42	51.84	51.84	49.87	46.32	38.75	51.18
Fe_2O_3	9.91	30.33	27.39	39.84	33.07	29.36	32.10	50.83	42.64	40.00	35.45	21.58	20.50	20.50	27.06	32.88	49.78	24.47
V_2O_3	0.22	0.43	0.47	0.84	0.67	0.62	0.81	0.69	1.12	0.80	0.37	0.42	0.39	0.39	0.58	1.17	1.03	0.71
MnO	2.32	1.33	1.35	0.76	0.94	0.99	0.95	0.36	0.47	0.56	1.14	1.61	1.84	1.84	0.98	0.63	0.31	0.84
Cr_2O_3	0.01	0.04	0.05	0.29	0.19	0.17	0.30	0.26	0.31	0.34	0.02	0.02	0.03	0.03	0.07	0.45	0.37	0.09
Total	99.22	99.61	98.30	98.53	98.96	98.90	99.25	99.95	99.38	99.60	98.77	99.10	99.28	99.28	99.94	98.97	99.22	99.98
Mg	0.001	0.001	0.002	0.001	0.001	0.001	0.002	0.000	0.003	0.001	0.000	0.002	0.001	0.001	0.001	0.001	0.002	0.002
Al	0.000	0.000	0.003	0.001	0.001	0.002	0.001	0.002	0.001	0.002	0.002	0.001	0.001	0.001	0.001	0.001	0.002	0.002
Ti	0.849	0.547	0.582	0.391	0.497	0.551	0.508	0.245	0.350	0.395	0.469	0.575	0.672	0.689	0.592	0.485	0.247	0.626
Fe^{2+}	1.765	1.481	1.515	1.332	1.438	1.494	1.448	1.195	1.295	1.344	1.407	1.507	1.602	1.613	1.538	1.432	1.194	1.575
Fe^{3+}	0.297	0.901	0.824	1.189	0.985	0.876	0.952	1.497	1.257	1.182	1.062	0.842	0.645	0.612	0.800	0.974	1.471	0.722
V	0.014	0.027	0.030	0.053	0.042	0.039	0.051	0.043	0.069	0.050	0.023	0.027	0.027	0.025	0.036	0.073	0.064	0.044
Mn	0.073	0.042	0.043	0.024	0.030	0.031	0.030	0.011	0.015	0.017	0.036	0.044	0.051	0.058	0.031	0.020	0.010	0.026
Cr	0.000	0.001	0.001	0.009	0.006	0.005	0.009	0.008	0.009	0.010	0.001	0.002	0.001	0.001	0.002	0.013	0.011	0.003
Total	3.000	3.000	3.000	3.000	3.000	3.000	3.000	3.000	3.000	3.000	3.000	3.000	3.000	3.000	3.000	3.000	3.000	3.000

Note: Gab = oxide-poor gabbro; Ore = oxide-rich gabbro; n = number of analysis.

Table 3 Average compositions (wt%) of ilmnite in gabbros from drill core Zk2801 in the intrusions from the Zhuqing area

Sample No.	ZK 2834	ZK 2830	ZK 2827	ZK 2825	ZK 2823	ZK 2822	ZK 2821	ZK 2818	ZK 2817	ZK 2816	ZK 2813	ZK 2811	ZK 2807	ZK 2806	ZK 2805	ZK 2804	ZK 2802	ZK 2801
Rock name	Gab	Gab	Gab	Ore	Ore	Ore	Ore	Ore	Ore	Ore	Gab	Gab	Gab	Gab	Ore	Ore	Ore	Ore
Unit	1	1	1	2	2	2	2	2	2	2	3	3	3	3	4	4	4	4
n	5	5	4	7	10	10	4	6	6	10	3	6	6	6	5	7	7	3
MgO	0.02	0.03	0.03	0.02	0.05	0.06	0.05	0.09	0.03	0.03	0.01	0.04	0.01	0.03	0.08	0.04	0.04	0.07
Al_2O_3	0.01	0.03	0.02	0.01	0.02	0.03	0.00	0.06	0.01	0.02	0.02	0.01	0.01	0.01	0.02	0.01	0.02	0.01
TiO_2	51.71	51.58	51.57	51.56	51.38	51.77	51.07	50.62	51.85	51.50	51.72	51.91	52.04	51.51	51.50	51.91	52.10	51.78
FeO	43.03	43.55	43.37	44.27	44.06	44.55	44.28	43.53	44.99	44.80	42.92	43.55	43.89	43.16	44.40	45.25	45.18	44.95
Fe_2O_3	1.12	1.21	0.92	1.13	1.28	1.17	1.84	1.70	1.29	1.25	0.89	0.94	0.97	1.18	1.12	0.78	0.41	0.60
V_2O_3	0.02	0.05	0.06	0.15	0.16	0.17	0.23	0.07	0.18	0.18	0.03	0.13	0.16	0.12	0.18	0.27	0.21	0.21
MnO	3.90	3.32	3.37	2.60	2.68	2.50	2.46	2.63	2.22	2.08	3.95	3.49	3.36	3.65	2.36	1.77	1.87	1.83
Total	99.81	99.77	99.34	99.73	99.62	100.24	99.92	98.70	100.58	99.85	99.54	100.06	100.45	99.65	99.65	100.04	99.83	99.44
Mg	0.000	0.000	0.000	0.000	0.000	0.000	0.000	0.001	0.000	0.000	0.000	0.001	0.000	0.000	0.001	0.001	0.001	0.002
Al	0.000	1.636	0.000	1.599	0.000	1.559	0.000	1.499	0.000	1.428	0.000	1.333	0.000	1.199	0.000	0.999	0.000	0.669
Ti	0.164	0.179	0.179	0.196	0.196	0.218	0.216	0.243	0.245	0.279	0.282	0.328	0.328	0.392	0.394	0.491	0.495	0.660
Fe^{2+}	0.152	0.168	0.168	0.187	0.187	0.209	0.208	0.233	0.236	0.270	0.260	0.306	0.307	0.365	0.378	0.476	0.478	0.637
Fe^{3+}	0.004	0.004	0.003	0.005	0.005	0.000	0.008	0.009	0.006	0.007	0.005	0.006	0.007	0.010	0.000	0.008	0.004	0.000
V	1.666	0.000	1.636	0.001	1.600	0.002	1.556	0.001	1.501	0.002	1.428	0.002	1.334	0.002	1.206	0.006	1.002	0.006
Mn	0.014	0.013	0.013	0.011	0.012	0.012	0.012	0.014	0.012	0.013	0.024	0.025	0.024	0.031	0.020	0.019	0.020	0.026
Total	2.000	2.000	2.000	2.000	2.000	2.000	2.000	2.000	2.000	2.000	2.000	2.000	2.000	2.000	2.000	2.000	2.000	2.000

Note: Gab = oxide-poor gabbro; Ore = oxide-rich gabbro; n = number of analysis.

microprobe wavelength-dispersive spectrometry at the State Key Laboratory of Lithospheric Evolution, Institute of Geology and Geophysics, CAS. The beam current was 20 nA with acceleration voltage of 15 kV and beam size of 1 μm. Both natural and synthetic standards were used for silicate and oxide minerals calibration.

4 Results

4.1 Clinopyroxene

Mg number ($Mg^{\#}$) ranges from 32.52 to 44.18 and from 50.18 to 58.97 for clinopyroxenes in the oxide-rich and oxide-poor gabbros, respectively. Clinopyroxenes had SiO_2 contents ranging from 51.49 to 55.54. Content of Al_2O_3 and TiO_2 vary from 0.64 to 2.35 wt% and from 0.013 to 0.19 wt%, respectively. The CaO content ranges from 11.34 % to 12.27 %, which positively correlated with $Mg^{\#}$ (Fig. 4a). In contrast, the MnO content (0.15–0.37 wt.%) increases with decreasing $Mg^{\#}$ (Fig. 4b), reflecting a fractionation trend (Charlier et al., 2009).

4.2 Fe–Ti oxides

Magnetites and ilmenites in the gabbros of the Zhuqing area have a wide range in composition (Table 2). Variable Ti content in magnetites was most likely caused by ilmenite exsolutions within the magnetites. Higher Ti content merely reflected the absence of large ilmenite exsolutions within these magnetites. However, the lower and variable Ti content of the magnetites is to variable amounts of coarse ilmenite exsolutions in the magnetites. V_2O_3 contents vary from 0.22 to 1.17 wt% and Cr_2O_3 contents from 0.01 to 0.45 wt% for magnetites in the

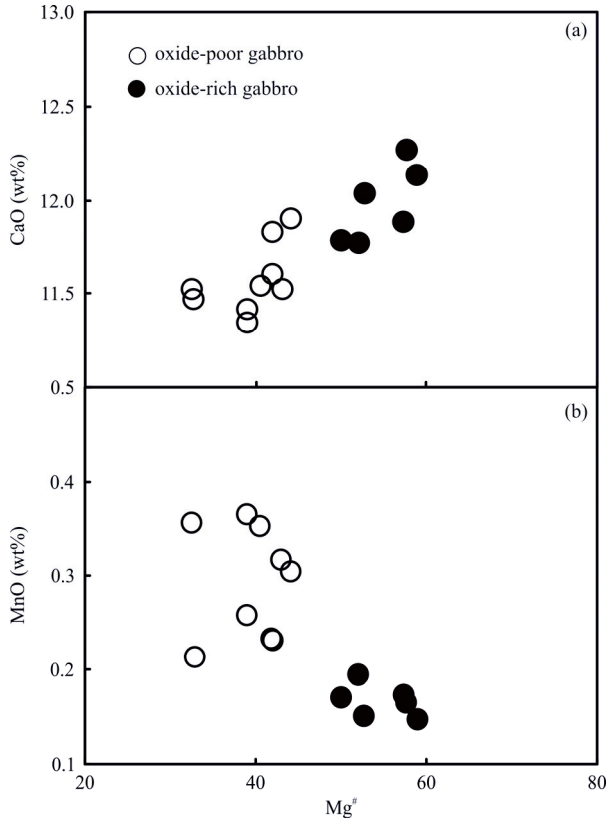

Fig. 4. Plots of $Mg^{\#}$ versus CaO (a) and MnO (b) for clinopyroxene in the intrusions in the Zhuqing area.

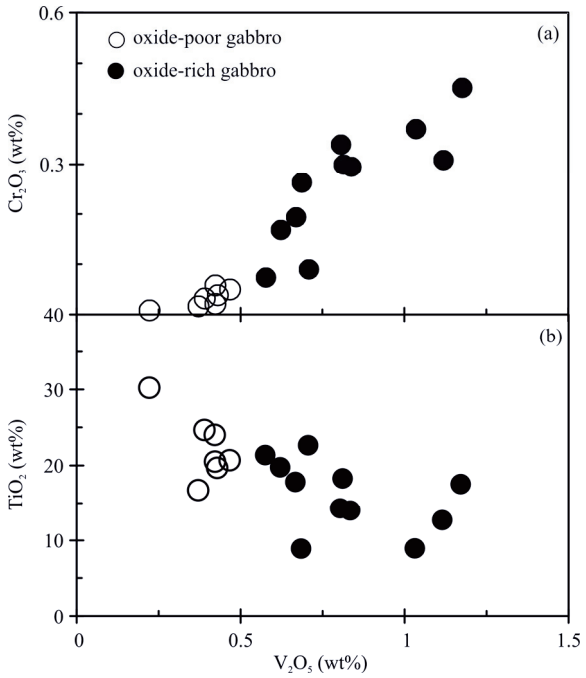

Fig. 5. Plots of V_2O_3 versus Cr_2O_3 (a) and TiO_2 (b) for magnetite in the intrusions in the Zhuqing area.

oxide-rich and oxide-poor gabbros, respectively. Cr_2O_3 and TiO_2 contents correlated well with V_2O_3 content in magnetite (Fig. 5). The ilmenites contain < 0.08 wt% MgO, <0.06 wt% Al_2O_3, and < 0.01 Cr_2O_3. TiO_2 content in the ilmenites range from 50.62 to 52.10 wt%, higher than that of pure ulvöspinel (Fe_2TiO_4, 36 wt%). The FeO / Fe_2O_3 ratios range from 24 to 57, with two exceptions (Fig. 6a). The FeO, MnO and V_2O_3 correlate well with TiO_2 (Fig. 6b–d).

5 Discussion

5.1 Unique mineral compositions

Compositional analyses of the samples for this study would not likely yield the original composition because the variable mineral composition in mafic intrusions could be modified not only by fractional crystallization but also by other processes, such as magma mixing, crystallization of trapped intercumulus liquid and sub-solidus re-equilibration between minerals (Barnes, 1986).

The sub-solidus re-equilibration could lead to redistribution of elements between oxide minerals and silicate mineral assemblage. Along with the decreasing temperatures, the Fe–Mg exchange would cause the Fe–Ti oxides to become poorer, and clinopyroxene richer in Mg content on cooling (Frost et al., 1988; Frost and Lindsley, 1991). The crystallization of trapped intercumulus liquid is also capable of forming overgrowths that, on equilibration of cumulus minerals, shifts their compositions to become more evolved in comparison with the original compositions (Barnes, 1986).

If this Fe–Mg exchange exists, the silicate minerals in most oxide-rich samples might be richer in Mg, causing the increasing $Mg^{\#}$ in clinopyroxene. In contrast, the mineral in the oxide-poor silicate rocks could yield a low Mg content. In the present study, the $Mg^{\#}$ in clinopyroxene is higher in the oxide-rich gabbros than those in the oxide-poor samples (Table 1, Fig. 7a). It seems that the exchange of Fe–Mg between magnetite and clinopyroxene during cooling stage existed. However, the CaO and MnO contents in clinopyroxene positively and negatively correlate with $Mg^{\#}$, respectively, suggesting that the clinopyroxene was originally fractionally crystalized from parental magma (Charlier et al., 2009) (Fig. 4). Furthermore, The MgO content in the Fe–Ti oxides of the Zhuqing gabbros is too low to process Fe^{2+}-Mg^{2+} exchange with clinopyroxene. As a result, the sub-solidus re-equilibration and the crystallization of trapped intercumulus liquid may not have significantly affected clinopyroxene in the Zhuqing gabbros, indicating that clinopyroxene and the Fe–Ti oxides in the gabbros of the Zhuqing area was mainly originally derived from parental magma rather than from Fe–Mg exchange with Fe–Ti oxides.

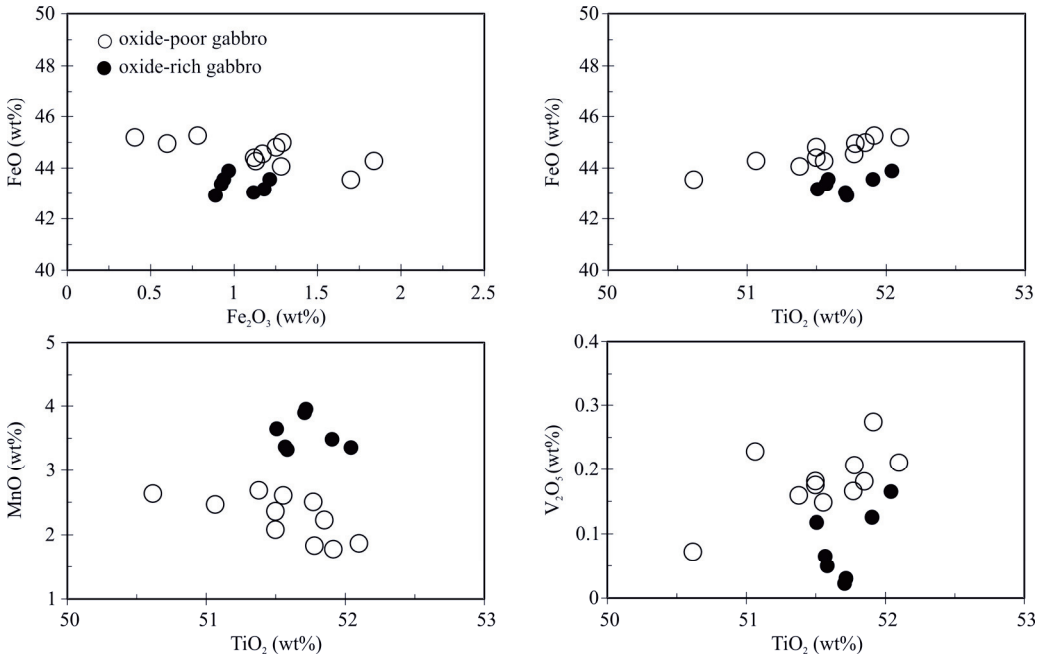

Fig. 6. Plots of Fe_2O_3 versus FeO (a) for magnetite; and TiO_2 versus FeO (b), MnO (c), and V_2O_3 (f) for ilmenite in the intrusions in the Zhuqing area.

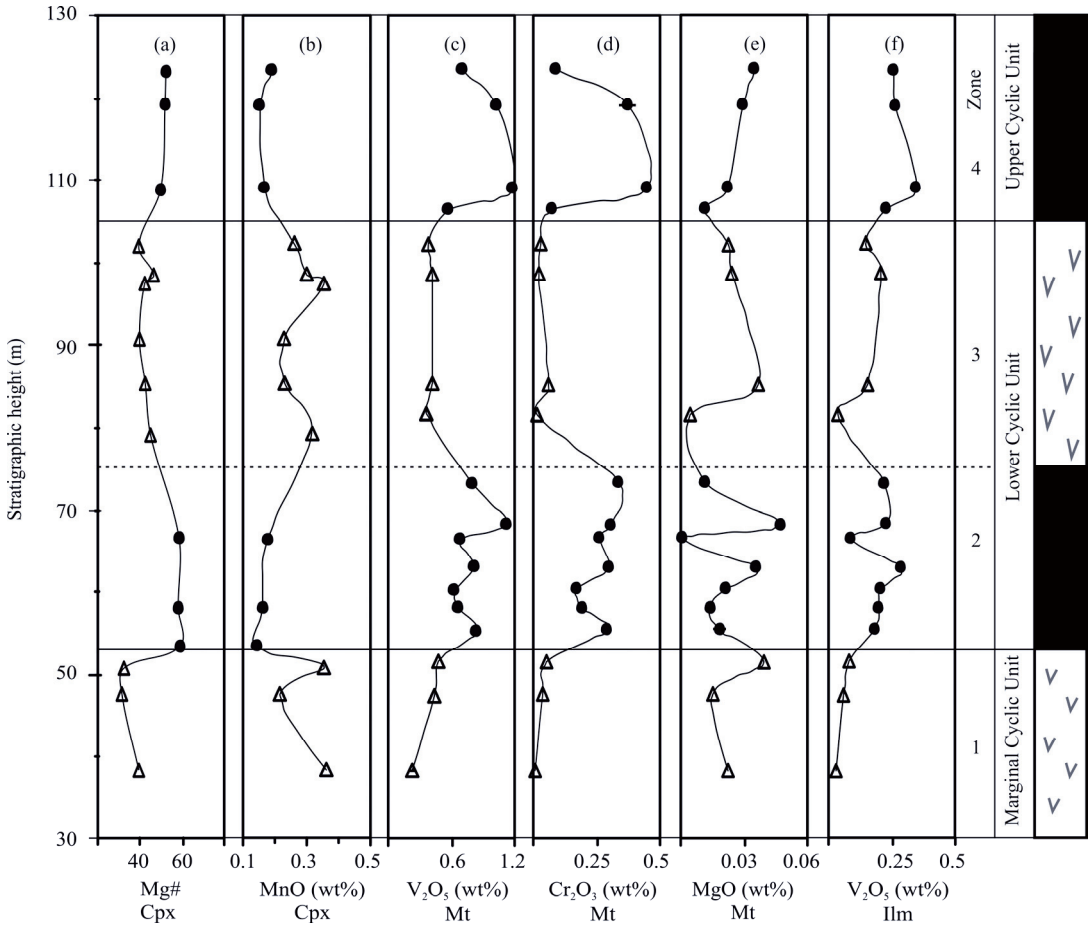

Fig. 7. Variations of $Mg^{\#}$ and MnO in clinopyroxene, V_2O_3, Cr_2O_3, and MgO in magnetite, and V_2O_3 in ilmenite across a profile through the intrusions in the Zhuqing area.

Compared to magnetites in other typical oxide-barring intrusions such as the Bushveld Complex (Reynolds, 1985a), the Skaergaard intrusion (Naslund, 1984), the Fedorivka intrusion (Duchesne et al., 2006) and the Suwalki anorthosite (Charlier et al., 2009), the magnetites in the Zhuqing gabbros have obviously lower Fe_2O_3, MgO and higher TiO_2 (Fig. 8). The ilmenites from the Zhuqing intrusions had much lower MgO and Fe_2O_3 but higher TiO_2 than those of the Bushveld Complex (Reynolds, 1985a), the Skaergaard intrusion (Naslund, 1984), the Fedorivka intrusion (Duchesne et al., 2006), and the Suwalki anorthosite (Charlier et al., 2009) (Fig. 9). The clinopyroxene (CPX) ($Mg^{\#}$ = 46) in the intrusions of the Zhuqing area were more evolved than other typical Fe–Ti oxide-rich complexes (Skaergaard intrusion: $Mg^{\#}$ = 65; McBirney., 1996; Bushveld Complex: $Mg^{\#}$ (Cpx) = 67; Tegner et al., 2006; Windimurra Complex: $Mg^{\#}$ (Cpx) = 67; Mathison and Ahmat, 1996).

Magnetites in the oxide-rich gabbros generally have relatively higher FeO, V_2O_3, MnO and Cr_2O_3 contents and lower Fe_2O_3 content than those in the oxide-poor gabbros (Fig. 7). Ilmenites in the oxide-rich gabbros have relatively higher FeO, V_2O_3, and MgO contents and lower MnO content than those in the oxide-poor gabbros (Fig. 7). The positive correlation between V_2O_3 and Cr_2O_3 contents in magnetite compositions (Fig. 5) is consistent with the compatible behavior of Cr and Ni in magnetite ($D_{Cr}^{Mt/liq}$ = 153, Rollinson, 1993; $D_{Ni}^{Mt/liq}$ = 31–65, Nielsen, 1992), suggesting that the higher Cr content of the oxide-rich gabbros relative to the oxide-poor gabbros was not only because the oxide-rich gabbros contained more magnetite but also because the magnetite was richer in Cr content. Mg numbers of clinopyroxenes from the oxide-rich gabbros were generally higher than those of clinopyroxenes from the oxide-poor samples (Fig. 7a). The $Mg^{\#}$ deceases whereas MnO increases from the base upward in the lower cyclic unit (Fig. 7a and 7b) which is consistent with fractional crystallization of the magma from the base to the top. This finding was further confirmed by the variations in mineral composition of the Fe–Ti oxides across the profile of the intrusions in the Zhuqing area (Fig. 7c–7f), suggesting that fractional crystallization and cumulative processes were responsible for the formation of the gabbros and magnetite layer in a single cycle.

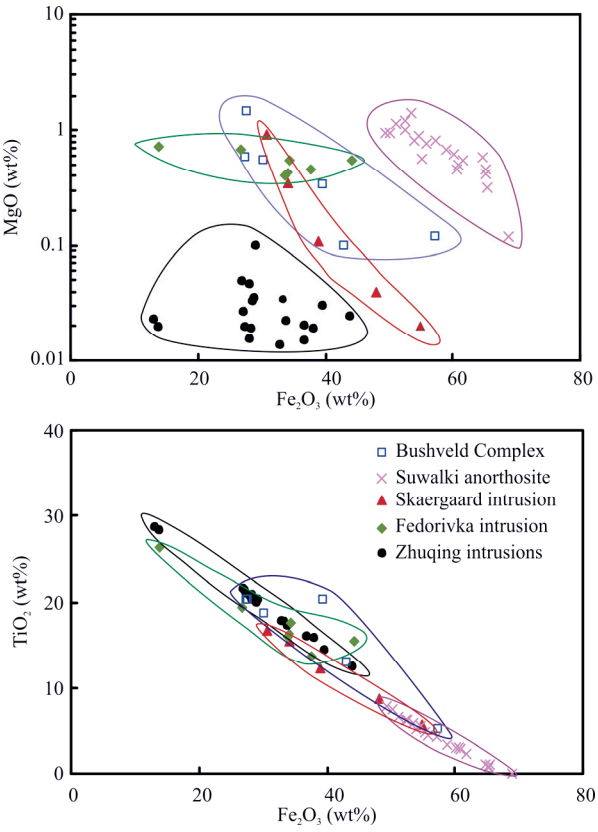

Fig. 8. Plots of Fe_2O_3 versus MgO and TiO_2 for magnetite in the Bushveld Complex (Reynolds, 1985a), the Suwalki anorthosite (Charlier et al., 2009), the Skaergaard intrusion (Naslund, 1984), the Fedorivka intrusion (Duchesne et al., 2006), and the intrusions in the Zhuqing area.

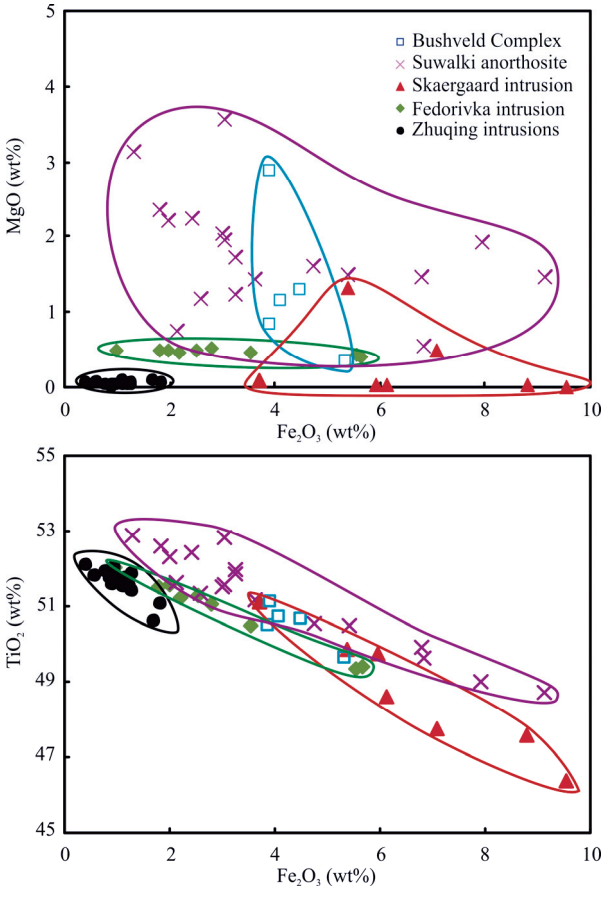

Fig. 9. Plots of Fe_2O_3 versus MgO and TiO_2 for ilmenite in the Bushveld Complex (Reynolds, 1985a), the Suwalki anorthosite (Charlier et al., 2009), the Skaergaard intrusion (Naslund, 1984), the Fedorivka intrusion (Duchesne et al., 2006), and the intrusions in the Zhuqing area.

5.2 Oxygen fugacity

Oxidation–exsolution of magnetite commonly involves the removal of Ti, Al and Mg to form ilmenite and spinel. Buddington and Lindsley (1964) interpreted magnetite$_{ss}$–ilmenite$_{ss}$ intergrowths as products of subsolidus oxidation–exsolution of pre-existing magnetite–ulvöspinel solid solutions. Exsolution patterns and fabrics vary with increasing degrees of oxidation and diffusion, resulting in a systematic series of microtextures from a single-phase homogeneous ulvöspinel grain, through trellis or sandwich intergrowths of ilmenite lamellae to granules of ilmenite within or on the external borders of magnetite. Experimental evidence has shown that oxidation affects the (magnetite–ulvöspinel)$_{ss}$ precursor crystals from the rim towards the core (Haggerty, 1991). Microtextures of magnetite in the Zhuqing Fe–Ti oxide ore deposits, for instance, presented ilmenite exsolutions in magnetite mostly at the rim, rather than the core (Fig. 3e–3f), indicating that they belonged to the oxidation–exsolution stage of trellis or sandwich intergrowths of ilmenite lamellae. Moreover, the trellis and sandwich textures of the magnetite with ilmenite lamellae from the Zhuqing intrusions were consistent with the features of an early stage which was classified by Haggerty (1991) on the basis of increasing oxidation. Observations based on the general exsolution sequence of microtextures for a primary magnetite–ulvöspinel solid solution during successive oxidation suggested a relatively low fO_2.

$D_V^{Mt/liq}$ decreases by approximately one order of magnitude with increasing fO_2 from NNO–0.7 to NNO+2.6 (Canil, 1999; Toplis and Corgne, 2002), and thus magnetite crystallizing early at high fO_2 is characterized by relative consistent V_2O_3 contents (Pang et al., 2010; Bai et al., 2012). The magnetites in all the samples from the Zhuqing Fe–Ti–V oxide ores have obviously higher V_2O_3 content than those in the oxide-poor gabbros (Fig. 7c), suggesting a relatively high V distribution coefficient between magnetite and silicate melts because of the absence of high fO_2 values in the rocks from the Zhuqing area. Therefore, the high fO_2 did not induce extensive magnetite crystallization at an early stage in the Zhuqing magma; on the contrary, the Fe–Ti oxide would be saturated in the residual magma after a lengthy Fenner trend period at relatively low fO_2 conditions.

Oxygen fugacities and the temperatures at which the minerals last equilibrated can be estimated based on compositions of magnetite and ilmenite pairs (Buddington and Lindsley, 1964; Andersen and Lindsley, 1985). We conducted calculations on magnetite–ilmenite mineral pairs using the ilmenite–magnetite geothermobarometry program ILMAT120 (Lepage, 2003) based on the geothermometer of Anderson and Lindsley (1985). The blocking temperatures and fO_2 of subsolidus equilibration ranged from 640 to 450 °C and from 27 to 24 ($-\lg fO_2$), respectively. This suggested that the end of subsolidus equilibration for magnetite and ilmenite of Zhuqing Fe–Ti oxide ores occurred at a low fO_2 condition, which was consistent with the above estimates based on mineral compositions and oxidation–exsolution textures of the Zhuqing samples.

5.3 Implications for petrogenesis and mineralization

Immiscible separation of Fe-rich liquids from silicate magmas has been proposed as an explanation for oxide ore body formation and the interstitial nature of the oxides in the host rocks (Lister, 1966; Philpotts, 1967; Reynolds, 1985a; Zhou et al., 2005; 2013; Dong et al., 2013; Wang and Zhou, 2013; Wang et al., 2013; Chai et al., 2014). Immiscible oxide melt would be denser than the silicate magmas from which they formed, and would likely percolate downward through the crystal-bearing silicate magma into the crystalmush at the base of the magma chamber. Abundant apatites associated with magnetites occur in anorthosite massifs as well as in layered intrusions (Philpotts, 1967; Kolker, 1982; Reynolds, 1985a; Nystroem and Henriquez, 1994). In particular, apatite-rich magnetite ores in anorthosite massifs, known as nelsonite, are thought to have formed from immiscible Fe-rich liquids (Naslund et al., 2002). Phosphorus usually plays a very important role in expanding the immiscibility field (Watson, 1976; Freestone, 1978; Visser and Koster van Groos, 1979; Ryerson and Hess, 1980). However, the lack of abundant apatites (Fan et al., 2013) in these Fe–Ti oxide ore horizons was against the immiscible model.

The formation of Fe–Ti oxide deposits was generally thought to result from the crystallization of magnetite and ilmenite during the late stage in mafic-ultramafic magmas (Reynolds, 1985a, b). However, it has been suggested that magnetite may crystallize at an early stage from magma at a relatively high fO_2 (Toplis and Caroll 1995; Ganino et al. 2008; Pang et al. 2010; Bai et al. 2012). The timing of crystallization of Fe–Ti oxides is a very important factor for the understanding of the magma differentiation mechanism of Fe–Ti oxide crystallization and accumulation but remains under debate.

The MgO content of ilmenite has no systematic variation in fO_2 changes (Toplis and Carroll., 1995; Botcharnikov et al., 2008) and the main controlling factor is probably the MgO content of the liquid. The ilmenites from the intrusions in the Zhuqing area had much lower MgO than those of the Bushveld Complex and the Skaergaard intrusion (Fig. 9). The clinopyroxene in the Zhuqing intrusion were more evolved than other typical Fe–Ti oxide-rich complexes (e.g., Skaergaard intrusion,

Bushveld Complex, Windimurra Complex). These characteristics may reflect that the Fe–Ti oxides from the Zhuqing intrusion crystallized at a relatively late stage of evolution from a more evolved magma.

As previously discussed, factors that could induce extensive magnetite crystallization at an early stage, such as high fO_2, were absent in the rocks from the Zhuqing area. Therefore, late-stage fractional crystallization of titanomagnetite and ilmenite from an evolved parental magma most likely resulted in the formation of Fe–Ti–V oxide deposits in the intrusions from the Zhuqing area.

Sharp reversals of mineral components (Fig. 7) between the boundaries of the cycles indicated that multiple pulses of magma replenishment in the magma chamber may have been involved in the formation of the Zhuqing oxide ore deposits because fractional crystallization and cumulative processes were only responsible for the formation of the Zhuqing gabbros and Fe–Ti oxide layer in a single cycle. Moreover, a new recharge of more Cr- and V-rich magma was also confirmed by the presence of higher Cr_2O_3 and V_2O_3 in magnetite from the base of each cycle (Table 2). Firstly, Fe–Ti oxide as well as clinopyroxene crystallized at the lowermost zone of the chamber due to the rapid cooling of the lowermost layer by heat loss to the overlying layer. Subsequently, during settling, sorting of these minerals due to the density contrast would form a Fe–Ti oxide ore layer and an overlying layer of mineralized silicates in the lower cycle. The primitive parental magma, enriched in Fe, Ti, Mg, Cr, and V, entered the magma chamber and spread out at the base of the upper cycle beneath the resident magma after the density of the residual magma decreased as a result of fractionation and removal of clinopyroxene and oxide minerals. The magma mixture underwent the same sequence of crystallization and sorting to form the upper Fe–Ti oxide layer with a silicate rock layer in the upper cycle. Therefore, both fractional crystallization and multiple magma recharge episodes played important roles in generating the Zhuqing Fe–Ti oxide rich layers.

6 Conclusions

The following conclusions were drawn from this study:

(1) Rocks of the mafic intrusions in the Zhuqing area did not have high oxygen fugacities based on the calculations; the relatively high V distribution coefficient between magnetite and silicate melts and the specific $magnetite_{ss}$–$ilmenite_{ss}$ intergrowths due to subsolidus oxidation–exsolution.

(2) The clinopyroxene, magnetite and ilmenite in the intrusions of the Zhuqing area have much lower MgO than those of other typical Fe–Ti oxide-rich complexes, indicating that the Fe–Ti oxides from the intrusion in the Zhuqing area crystallized at a relatively late stage of evolution from a more evolved magma.

(3) Sharp reversals occur in Fe–Ti oxides and clinopyroxene at the boundary between the upper and lower cycles of the intrusions in the Zhuqing area, suggesting multiple episodes of magma recharge during magma evolution.

Acknowledgements

We appreciate the assistance of Prof. G.F. Zhou, Q. Mao, Y.G. Ma and Ms. W.Q. Zheng for assistance with EMPA. The paper has benefited from constructive comments of two anonymous reviewers and the editor. This work is supported by the National Natural Science Foundation of China (Grants 41403044, 41273049, 41572074).

Manuscript received July 10, 2015
accepted Sept. 8, 2015
edited by Fei Hongcai

References

Anderson, A.T., and Lindsley, D.H., 1985. Model for the Ti magnetite or ilmenite geothermometers and oxygen barometers (Abstract). *Eos, Transactions, American Geophysical Union*, 66: 416.

Bai, Z.J., Zhong, H., Naldrett,A.J., Zhu, W.G., and Xu, G.W., 2012. Whole-rock and mineral composition constraints on the genesis of the giant Hongge Fe–Ti–V oxide deposit in the Emeishan large igneous province, southwest China. *Economic Geology*, 107: 507–524.

Barnes, S.J., 1986. The effect of trapped liquid crystallization on cumulus mineral compositions in layered intrusions. *Contributions to Mineralogy and Petrology*, 93: 524–531.

Botcharnikov, R.E., Almeev, R.R., Koepke, J., and Holtz, F., 2008. Phase relations and liquid lines of descent in hydrous ferrobasalt--Implications for the Skaergaard intrusion and Columbia River flood basalts. *Journal of Petrology*, 49: 1687–1727.

Buddington, A.F., and Lindsley, D.H., 1964. Iron–titanium oxide minerals and synthetic equivalents. *Journal of Petrology*, 5: 310–357.

Canil, D., 1999. Vanadium partitioning between orthopyroxene, spinel and silicate melt and the redox states of mantle source regions for primary magmas. *Geochimica et Cosmochimica Acta*, 63: 557–572.

Chai Fengmei, Yang Fuquan, Li Qiang, Zang Mei, Geng Xinxia and Meng Qingpeng, 2014. Metallogenic mechanism of the Abagong apatite-rich iron deposit in Altay, Xinjiang: evidence from inclusions and stable isotopes. *Acta Petrological Sinica*, 50(5): 1397–1414 (in Chinese with English abstract).

Chang Xiangyang, Zhu Bingquan, Sun Dazhong, Qiu Huaning and Zou Ri, 1997. Isotope geochemistry study of Dongchuan copper deposits in Middle Yunnan Province, SW China: stratigraphic chronology and application of geochemical

exploration by lead isotopes. *Geochimica*, 26: 32–38 (in Chinese with English abstract).

Charlier, B., Duchesne, J.C., and Auwera, J.V., 2006. Magma chamber processes in the Tellnes ilmenite deposit (Rogaland anorthosite province, SW Norway) and the formation of Fe-Ti ores in massif-type anorthosites. *Chemical Geology*, 234: 264–290.

Charlier, B., Namur, O., Duchesne, J.C., Wiszniewska, J., Parecki, A. and Auwera, J.V., 2009. Cumulate origin and polybaric crystallization of Fe-Ti oxide ores in the Suwalki anorthosite, northeastern Poland. *Economic Geology*, 104: 205–221.

Dong Huan, Xing Changming and Wang Christina Yan, 2013. Textures and mineral compositions of the Xinjie layered intrusion, SW China: implications for the origin of magnetite and fractionation process of Fe–Ti-rich basaltic magmas. *Geoscience Frontiers*, 4: 503–515.

Duchesne, J.C., Shumlyanskyy, L., and Charlier, B., 2006. The Fedorivka layered intrusion (Korosten Pluton, Ukraine): An example of highly differentiated ferrobasaltic evolution. *Lithos*, 89: 353–376.

Fan, H.P., Zhu, W.G., Li, Z.X., Zhong, H., Bai, Z.J., He, D.F., Chen, C.J., and Cao, C.Y., 2013. Ca. 1.5 Ga mafic magmatism in South China during the break-up of the supercontinent Nuna/Columbia: The Zhuqing Fe–Ti–V oxide ore-bearing mafic intrusions in western Yangtze Block, *Lithos*, 168-169: 85-98.

Freestone, I., 1978. Liquid immiscibility in alkali-rich magmas. *Chemical Geology*, 23: 115-123.

Frost, B.R., Lindsley, D.H., and Andersen, D.J., 1988, Fe-Ti oxide-silicate equilibria; assemblages with fayalitic olivine: *American Mineralogist*, 73: 727–740.

Frost, B.R., and Lindsley, D.H., 1991. Occurrence of iron–titanium oxide in igneous rocks. In: Lindsley, D.H. (Ed.), *Oxide Minerals: Petrologic and Magnetic Significance*. Mineralogical Society of America, 25: 433–468.

Ganino, C., Arndt, N.T., Zhou, M.F., Gaillard, F., and Chauvel, C., 2008. Interaction of magma with sedimentary wall rock and magnetite ore genesis in the Panzhihua mafic intrusion, SW China. *Mineralium Deposita*, 43: 677–694.

Ganino, C., Arndt, N.T., Chauvel, C., Jean, A., and Athurion, C., 2013a. Melting of carbonate wall rocks and formation of the heterogeneous aureole of the Panzhihua intrusion, China. *Geoscience Frontiers*, 4: 535–546.

Ganino, C., Harris, C., Arndt, N.T., Prevec, S.A., and Howarth, G.H., 2013b. Assimilation of carbonate country rock by the parent magma of the Panzhihua Fe–Ti–V deposit (SW China): evidence from stable isotopes. *Geoscience Frontiers*, 4: 547–554.

Gao Shan, Qiu Yumin, Ling Wenli, McNaughton, N.J., and Groves, D.I., 2001. Single zircon U-Pb dating of the Kongling high-grade metamorphic terrain: Evidence for >3.2 Ga old continental crust in the Yangtze craton. *Science in China Series D*, 4: 326–335.

Geng Yuansheng, Yang Chonghui, Du Lilin, Wang Xinshe, Ren Liudong and Zhou Xiwen, 2007. Chronology and tectonic environment of the Tianbaoshan formation: new evidence from zircon SHRIMP U-Pb age and geochemistry. *Geological Review*, 53: 556–563 (in Chinese with English abstract).

Greentree, M.R., and Li, Z.X., 2008. The oldest known rocks in south-western China: SHRIMP U-Pb magmatic crystallization age and detrital provenance analysis of the Paleoproterozoic Dahongshan Group. *Journal of Asian Earth Sciences*, 33: 289–302.

Greentree, M.R., Li, Z.X., Li, X.H., and Wu, H.C., 2006. Late Mesoproterozoic to earliest Neoproterozoic basin record of the Sibao orogenesis in western South China and relationship to the assembly of Rodinia. *Precambrian Research*, 151: 79–100.

Haggerty, S.E., 1991. Oxide textures—a mini-atlas. In: Lindsley, D.H. (ed.), *Oxide Minerals: Petrologic and Magnetic Significance*. Mineralogical society of America, 25: 129–220.

He Defeng, 2009. *Petrological and geochemical characteristics of the Lala copper deposit in Sichuan Province*. Beijing: Gradute School of the Chinese Academy of Sciences (Ph. D thesis): 1–103 (in Chinese with English abstract).

Hou Lin, D Jun, D Jun, Liao Zhenwen and Peng Huijuan, 2013. Zircon LA-ICP-MS dating of the magmatic breccia from the Yinachang iron-copper deposit in Wuding Country of Yunnan Province and its geological significance. *Geological Bulletin of China*, 32(4):580–588 (in Chinese with English abstract).

Howarth, G.H., and Prevec, S.A., 2013. Hydration versus oxidation:modeling implications for Fe–Ti oxide crystallization in mafic intrusions, with specific reference to the Panzhihua Intrusion, SW China. *Geoscience Frontiers*, 4: 555–569.

Howarth, G.H., Prevec, S.A., and Zhou Meifu, 2013. Timing of Ti–magnetite crystallization and silicate disequilibrium at the Panzhihua mafic layered intrusion: implications for ore forming processes. *Lithos*, 170–171: 73–89.

Irvine, T.N., 1988. Muskox Intrusion, Northwest Territories. In: Hulbert, L.J., Duke, J.M., Eckstrand, O.R., Lydon, J.W., Scoates, R.F.J., and Cabri, L.J. (eds.), *Geological environments of the platinum-group elements*. Geological Survey of Canada, Open File, 1440: 25–39.

Kolker, A., 1982. Mineralogy and geochemistry of Fe–Ti oxide and apatite (nelsonite) deposits and evaluation of the liquid immiscibility hypothesis. *Economic Geology*, 77, 1146–1158.

Lepage, L.D., 2003. ILMAT: an Excel worksheet for ilmenite–magnetite geothermometry and geobarometry. *Computer Geoscience*, 29: 673–678.

Li, Z.X., Wartho, J.A., Occhipinti, S., Zhang Chuanlin, Li Xianhua, Wang Jian, and Bao chaomin, 2007. Early history of the eastern Sibao orogen (South China) during the assembly of Rodinia: new $^{40}Ar/^{39}Ar$ dating and U–Pb SHRIMP detrital zircon provenance constraints. *Precamb Research*, 159: 74–94.

Lister, G.F., 1966. The composition and origin of selected iron-titanium deposits. *Economic Geology*, 61, 275-310.

Mathison, C.I., and Ahmat, A.L., 1996. The Windimurra Complex, Western Australia. In: Cawthorn R.G., (ed.), *Layered Intrusions*. Elsevier, 485–510.

McBirney, A.R., 1996. The Skaergaard Intrusion. In: Cawthorn R.G., (Ed.), *Layered Intrusions*. Elsevier, 147-180.

Mou Chuanlong, Lin Shiliang, and Yu Qian, 2003. The U-Pb ages of the volcanic rock of the Tianbaoshan formation, Huili, Sichuan province. *Journal of Stratigraphy*, 27: 216–219 (in Chinese with English abstract).

Naslund, H.R., 1984. Petrology of the Upper Border Series of the Skaergaard intrusion. *Journal of Petrology*, 25: 185–212.

Naslund, H.R., Henriquez, F., Nystrom, J.O., Vivallo, W., and Dobbs, F., 2002. Magmatic iron ores and associated

mineralization: examples from the Chilean High Andes and Coastal Cordillera. In: Porter, T.M. (Ed.), *Hydrothermal Iron Oxide Copper–Gold and Related Deposits: a Global Perspective*. Porter Geoconsultancy Pty. Ltd., vol. 2. PGC Publishing, Adelaide, South Australia, 207–228.

Nielsen, R., 1992. BIGD. FOR: a fortran program to calculate trace-element partition coefficients for natural mafic and intermediate composition magmas. *Computers and Geosciences*, 18: 773–788.

Nystroem, J.O., and Henriquez, F., 1994. Magmatic features of iron ores of the Kiruna type in Chile and Sweden; ore textures and magnetite geochemistry. *Economic Geology*, 89: 820–839.

Pang, K.N., Li, C., Zhou, M.F., and Ripley, E., 2008a. Abundant Fe-Ti oxide inclusions in olivine from the Panzhihua and Hongge layered intrusions, SW China: evidence for early saturation of Fe-Ti oxides in ferrobasaltic magma. *Contributions to Mineralogy and Petrology*, 156: 307–321.

Pang, K.N., Zhou, M.F., Qi, L., Shellnutt, J.G., Wang, C.Y., and Zhao, D.G., 2010. Flood basalt-related Fe–Ti oxide deposits in the Emeishan large igneous province, SW China. *Lithos*, 119: 123–136.

Pêcher, A., Arndt, N.T., Bauville, A., Zhou, M.F., Ganino, C., 2013. Structure of the Panzhihua Fe–Ti–V deposit, *China. Geosci. Front.,* 4: 571–581.

Peng Min, Wu Yuanbao, Wang Jing, Jiao Wenfang, Liu Xiaochi, and Yang SaiHong, 2009. Paleoproterozoic mafic dyke from Kongling terrain in The Yangtze Craton and its implication. *Chinese Science Bulletin*, 54(6): 1098–1104.

Philpotts, A.R., 1967. Origin of certain iron-titanium oxide and apatite rocks. *Economic Geology*, 62: 303–315.

Reynolds, I.M., 1985a. Contrasted mineralogy and textural relationships in the uppermost titaniferous magnetite layers of the Bushveld Complex in the Bierkraal area north of Rustenburg. *Economic Geology*, 80: 1027-1048.

Reynolds, I.M., 1985b. The nature and origin of titaniferous magnetite-rich layers in the Upper Zone of the Bushveld Complex: a review and synthesis. *Economic Geology*, 80: 1089–1108.

Rollinson, H., 1993. *Using geochemical data: evaluation, presentation, interpretation*. New York: Longman Scientific & Technical, 108.

Ryerson, F., and Hess, P., 1980. The role of P_2O_5 in silicate melts. *Geochimica et Cosmochimica Acta*, 44: 611–624.

Shi Yu, Wang Yuwang, Wang Jingbin, Li Dedong and Gao Yihan, 2014. Composition of titanomagnetite and microstructure of banded type ore in weiya fe-v-ti oxide deposits and its implication on metallogenesis. *Acta Geologica Sinica* (English edition), 88(s2): 310–311.

Song Hao, and Song Shiwei, 2015. Re-Os dating of chalcopyrite from the Lala IOCG depositt in the Kangdian copper belt, China. *Acta Geologica Sinica* (English edition), 89(2): 689–690.

Sun, W.H., Zhou, M.F., Gao, J.F., Yang, Y.H., Zhao, X.F., and Zhao, J.H., 2009. Detrital zircon U-Pb geochronological and Lu-Hf isotopic constraints on the Precambrian magmatic and crustal evolution of the western Yangtze block, SW China. *Precambrian Research*, 172: 99–126.

Tegner, C., Cawthorn, R.G., and Kruger, F.J., 2006. Cyclicity in the Main and Upper Zones of the Bushveld Complex, South Africa: Crystallization from a zoned magma sheet. *Journal of Petrology*, 47: 2257–2279.

Toplis, M.J., and Carroll, M.R., 1995. An experimental study of the influence of oxygen fugacity on Fe-Ti oxide stability, phase relations, and mineral-melt equilibria in ferro-basaltic systems. *Journal of Petrology*, 36: 1137–1170.

Toplis, M.J., and Corgne, A., 2002. An experimental study of element partitioning between magnetite, clinopyroxene and iron-bearing silicate liquids with particular emphasis on vanadium. *Contributions to Mineralogy and Petrology*, 144: 22–37.

Veksler, I.V., Dorfman, A.M., Borisov, A.A., Wirth, R., and Dingwell, D.B., 2007. Liquid immiscibility and the evolution of basaltic magma. *Journal of Petrology*, 48: 2187–2210.

Visser, W., and Koster van Groos, A.F., 1979. Effects of P_2O_5 and TiO_2 on liquid-liquid equilibria in the system K_2O-FeO-Al_2O_3-SiO_2. *American Journal of Science*, 279: 970–988.

Wang, C.Y., and Zhou, M.F., 2013. New textural andmineralogical constraints on the origin of the Hongge Fe–Ti–V oxide deposit, SW China. *Mineral Deposita*, 48: 787–798.

Wang, C.Y., Zhou, M.F., and Zhao, D.G., 2008. Fe-Ti-Cr oxides from the Permian Xinjie mafic-ultramafic layered intrusion in the Emeishan large igneous province, SW China: Crystallization from Fe- and Ti-rich basaltic magmas. *Lithos*, 102: 198–217.

Wang Kun, Xing Changming, Ren Zhongyuan and Wang Yan, 2013. Liquid immiscibility in the Panzhihua mafic layered intrusion: Evidence from melt inclusions in apatite. *Acta Petrological Sinica*, 29(10): 3503–3518 (in Chinese with English abstract).

Wang, L.J., Griffin, W.L., Yu, J.H., and O'Reilly, S.Y., 2013. U-Pb and Lu-Hf isotopes in detrital zircon from Neoproterozoic sedimentary rocks in the northern Yangtze Block: Implications for Precambrian crustal evolution. *Gondwana Research*, 23: 1261–1272.

Watson, E.B., 1976. Two-liquid partition coefficients: Experimental data and geochemical implications. *Contributions to Mineralogy and Petrology*, 56: 119–134.

Xing Changming, Wang Christina Yan and Zhang Mingjie, 2012. Volatile and C-H-O isotopic compositions of giant Fe-Ti-V oxide deposits in the Panxi region and their implica-tions for the sources of volatiles and the origin of Fe-Ti oxide ores. *Science China Earth Science*, 55: 1782–1795.

Yan, D.P., Zhou, M.F., Song, H.L., Wang, X.W., and Malpas, J., 2003. Origin and tectonic significance of a Mesozoic multi-layer over-thrust within the Yangtze Block (South China). *Tectonophysics*, 361: 239-254.

Yan, Hong, Liu Fulai, Du Lilin, Liu Pinghua and Wang Fang, 2012. Zircon U-Pb dating for metavolcanites in the Laochanghe Formation of the Dahongshan Group in southwestern Tangtze Block, and its geological significance. *Acta Petrologica Sinica*, 28(9): 2994–3014 (in Chinese with English abstract).

Yang, Yaomin, Tu Guanzhi, Hu Ruizhong and Shi Xuefa, 2005. Sm-Nd isotopic geochronology of the Yinachang Fe-Cu-REE deposit at Wuding, Yunnan Province and its genetic significance. *Chinese Science Bulletin*, 50(12): 1253–1258.

Ye Xiantao, Zhu Weiguang, Zhong Hong, He Defeng, Ren Tao, Bai Zhongjie and Hu Wenjun, 2013. Zircon U-Pb and chalcopyrite Re-Os geochronology, REE geochemistry of the Yinachang Fe-Cu-REE deposit in Yunnan Province and its

geological significance. *Acta Petrologica Sinica*, 29(4): 1167–1186 (in Chinese with English abstract).

Yin Fuguang., Sun Zhiming and Zhang Zhang, 2011. Mesoproterozoic stratigraphic-structure framework in Huili-Dongchuan area. *Geology Review*, 57, 770–778 (in Chinese with English abstract).

Zhang Chuanheng, Gao Linzhi, Wu zhenjie, Shi Xiaoying, Yan Quanren and Li Dajian, 2007. SHRIMP U-Pb zircon age of tuff from the Kunyang Group in central Yunnan: Evidence for Grenvillian orogeny in south China. *Chinese Science Bulletin*, 52: 1517–1525.

Zhao, X.F., and Zhou, M.F., 2011. Fe–Cu deposits in the Kangdian region, SW China: a Proterozoic IOCG (iron–oxide–copper–gold) metallogenic province. *Mineralium Deposita*, 46: 731–747.

Zhao, X.F., Zhou, M.F., Li, J.W., Sun, M., Gao, J.F., Sun, W.H., and Yang, J.H., 2010. Late Paleoproterozoic to early Mesoproterozoic Dongchuan Group in Yunnan, SW China: implications for tectonic evolution of the Yangtze Block. *Precambrian Research*, 182: 57–69.

Zheng, J.P., Griffin, W.L., O'Reilly, S.Y., Zhang, M., Pearson, N., and Pan, Y.M., 2006. Widespread Archean basement beneath the Yangtze Craton. *Geology*, 34: 417–420.

Zhou, M.F., Arndt, N.T., Malpas, J., Wang, Y., and Kennedy, A.K., 2008. Twomagma series and associated ore deposit types in the Permian Emeishan large igneous province, SW China. *Lithos*, 103: 352–368.

Zhou Meifu, Chen Terry Wei, Wang Christina Yan, Prevec, S.A., Liu Pingping, and Howarth, G.H., 2013. Two stages of immiscible liquid separation in the formation of Panzhihua-type Fe-Ti-V oxide deposits, SW China. *Geoscience Frontiers*, 4: 481–502.

Zhou, M.F., Robinson, P.T., Lesher, C.M., Keays, R.R., Zhang, C.J., and Malpas, J., 2005. Geochemistry, petrogenesis and metallogenesis of the Panzhihua gabbroic layered intrusion and associated Fe-Ti-V oxide deposits, Sichuan province, SW China. *Journal of Petrology*, 46: 2253–2280.

Zhou, M.F., Zhao, X.F., Chen, W., Li, X.C., Wang, W., Yan, D.P., and Qiu, H.N., 2014. Proterozoic Fe-Cu metallogeny and supercontinental cycles of the southwestern Yangtze Block, southern China and northern Vietnam. *Earth-Science Reviews*, 139: 59–82.

About the first author

FAN Hongpeng Male; born in 1987 in Anqing City, Anhui Province; doctor; associate research fellow in the State Key Laboratory of Ore Deposit Geochemistry, Institute of Geochemistry, Chinese Academy of Sciences; He is now interested in the study on Paleo- to Mesoproterozoic magmatism and associated ore deposit on the Western Margin of the Yangtze Block. Email:fanhongpeng@vip.gyig.ac.cn; phone: 15285086103.